Spreading of Liquid Drops over Thick Porous Layers: Complete Wetting Case

V. M. Starov,*,† S. A. Zhdanov,† and M. G. Velarde‡

Department of Chemical Engineering, Loughborough University, Loughborough, Leicestershire, LE11 3TU, U.K., and Instituto Pluridisciplinar, Universidad Complutense, Paseo Juan XXIII, n.1, 28040 Madrid, Spain

Received March 20, 2002. In Final Form: September 19, 2002

The spreading of small silicone oil drops (capillary regime of spreading) over various dry thick porous substrates (permeable in both normal and tangential directions) was experimentally investigated. The time evolution of the radii of both the drop base and the wetted region on the surface of the porous substrate was monitored. It was observed that the total duration of the spreading process can be divided into two stages: a first stage, when the drop base expands until its maximum value is reached, and a subsequent second stage, when the drop base shrinks. It was found that the dynamic contact angle remains constant during the second stage of spreading. The latter fact has nothing to do with the contact angle hysteresis, as there is no hysteresis in the system. Appropriate scales are used, with a dimensionless time, to plot the dimensionless radii of the drop base and of the wetted circle on the surface of the porous substrate, the relative dynamic contact angle, and the effective contact angle inside the porous substrate. All these experimental data fell onto universal curves when the spreading of different silicone oils is done on porous substrates of similar pore size and porosity.

Introduction

The spreading of liquids over solid surfaces is a fundamental process occurring in multiple applications such as coating, printing, and painting. The spreading over smooth homogeneous surfaces has been considered,[1−6] and it has been established that the singularity at the three-phase contact line is removed by the action of surface forces.[5,6] However, the vast majority of solid surfaces are rough to a varying degree, and in many cases surfaces are either porous or covered with a thin porous sublayer. The presence of roughness and/or a porous sublayer changes the wetability of the substrate[7] and, hence, the spreading conditions.[8−10] The theoretical description of spreading over real surfaces is usually done using an ad hoc empirical "slippage condition".[11−15]

The spreading of small liquid drops over thin porous layers saturated with the same liquid[16] or a dry porous layer[17] has been considered by appropriately matching flows in both the spreading drop and the porous substrate. For the description of liquid flows in porous substrates see refs 18 and 19.

In ref 17, the spreading of silicone oil drops over various dry microfiltration membranes (permeable in both normal and tangential directions) was discussed. Upon plotting of the dimensionless radii of the drop base and of the wetted region inside the porous layer using a dimensionless time, all experimental data fell on two universal curves. According to theory[17] (i) the dynamic contact angle dependence on the same dimensionless time should be a universal function and (ii) the dynamic contact angle should change rapidly over an initial short spreading stage and should remain constant over the remaining duration of the spreading process. The latter fact has nothing to do with contact angle hysteresis, as there was no hysteresis in the system under consideration in ref 17. These conclusions were in good agreement with experimental observations.[17]

In the present paper we extend our previous study[17] to the spreading of small silicone oil drops (capillary spreading regime) over different porous substrates whose thickness is much bigger than the drop size. A number of similarities with the case of the spreading over thin porous substrates[17] is found.

Theory

Assuming below that during the spreading over porous substrate the liquid drops remains spherical[17] (see Figure 1) we have

$$h(t,r) = \frac{2V_d}{\pi L^4}(L^2 - r^2), \quad r < L(t) \tag{1}$$

where $V_d(t)$ is the drop volume, $h(t,r)$ is the drop profile, L is the radius of the drop basis, and r is the radial coordinate.

†Loughborough University
‡ Universidad Complutense
* To whom correspondence should be addressed.

(1) Starov, V. M. *Colloid J.* **1983**, *45* (6), 1154 .
(2) de Gennes, P. G. *Rev. Mod. Phys.* **1985**, *57*, 827.
(3) Blake, T. D.; Hayenes, J. M. *J. Colloid Interface Sci.* **1969**, *30*, 421.
(4) Joanny, J.-F. *J. Mec. Theor. Appl.* **1986**, *5*, 249.
(5) Teletzke, G. F.; Davis, T. H.; Scriven, L. E. *Chem. Eng. Commun.* **1987**, *55*, 41.
(6) Starov, V. M.; Kalinin, V. V.; Chen, J.-D. *Adv. Colloid Interface Sci.* **1994**, *50*, 187.
(7) Tanigichi, M.; Pieracci, J.; Belfort, G. *Langmuir* **2001**, *17*, 4312.
(8) Raphael, E.; de Gennes, P. G. *C. R. Seances Acad. Sci. Paris* **1999**, *327*, Ser. II b, 685.
(9) Bacri, L.; Brochard, F. *Eur. Phys. J. E* **2000**, *3*, 87.
(10) Aradian, A., Raphael, E.; de Gennes, P. G. *Eur. Phys. J. E* **2000**, *2*, 367.
(11) Beaverse, G.; Johns, D. *J. Fluid Mech.* **1967**, *30*(1), 197.
(12) Greenspan, H. P. *J. Fluid Mech.* **1978**, *84*, 125.
(13) Neogi, P.; Miller, C. A. *J. Colloid Interface Sci.* **1983**, *92* (2), 338.
(14) Davis, S. H.; Hocking, L. M. *Phys. Fluids* **1999**, *11* (1), 48.
(15) Davis, S. H.; Hocking, L. M. *Phys. Fluids* **2000**, *12* (7), 1646.
(16) Starov, V. M.; Kosvintsev, S. R.; Sobolev, V. D.; Velarde, M. G.; Zhdanov, S. A. *J. Colloid Interface Sci.* **2002**, *246*, 372−379.
(17) Starov, V. M.; Kosvintsev, S. R.; Sobolev, V. D.; Velarde, M. G.; Zhdanov, S. A. *J. Colloid Interface Sci.* **2002**, *252*, 397−408.
(18) Marmur, A. *J. Colloid Interface Sci.* **1988**, *124*, 301.
(19) Borhan, A.; Rungta, K. K. *J. Colloid Interface Sci.* **1993**, *158*, 403.

10.1021/la025759y CCC: $22.00
Published on Web 11/02/2002

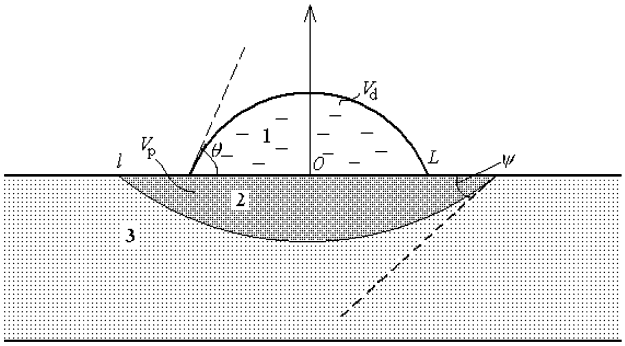

Figure 1. Spreading of liquid drops over dry porous substrates: (1) spherical drop, (2) wetted region inside the porous substrate (modeled by a spherical cap), (3) dry part of the porous substrate; $L(t)$, radius of the drop base; $l(t)$, radius of the wetted circle on the surface of the porous substrate; $\theta(t)$, dynamic contact angle of the spreading drop; $\psi(t)$, effective contact angle inside the porous substrate.

Equation 1 gives the following value of the dynamic contact angle, θ ($\tan\theta \approx \theta$)

$$\theta = 4V_d/\pi L^3 \tag{2}$$

hence,

$$L = (4V_d/\pi\theta)^{1/3} \tag{3}$$

The spreading process is a superposition of two motions: (i) the spreading of the drop over the already saturated part of the surface of the porous substrate, which results in an expansion of the drop base, and (ii) the shrinkage of the drop base caused by the imbibition into the porous substrate. Hence, we can write the following balance equation

$$dL/dt = v_+ - v_- \tag{4}$$

where v_+ and v_- denote unknown velocities of the expansion and the shrinkage of the drop base, respectively.

Using (3) we get the following:

$$\frac{dL}{dt} = -\frac{1}{3}\left(\frac{4V_d}{\pi\theta^4}\right)^{1/3}\frac{d\theta}{dt} + \frac{1}{3}\left(\frac{4}{\pi V_d^2\theta}\right)^{1/3}\frac{dV_d}{dt} \tag{5}$$

Over the whole duration of the spreading over the porous layer, both the contact angle and the drop volume can only decrease with time. Accordingly, the first term in the right-hand side of eq 5 is positive, and the second one is negative.

Comparison of eq 4 and 5 yields

$$v_+ \equiv -\frac{1}{3}\left(\frac{4V_d}{\pi\theta^4}\right)^{1/3}\frac{d\theta}{dt} > 0 \tag{6}$$

$$v_- \equiv -\frac{1}{3}\left(\frac{4}{\pi V_d^2\theta}\right)^{1/3}\frac{dV_d}{dt} > 0$$

Let $l(t)$ be the radius of the wetted region on the surface of the porous substrate. This unknown quantity cannot be determined without the numerical integration of Darcy equations inside the porous substrate and coupling with the flow in the drop. However, we can draw some conclusion based on the analysis given in ref 17. According to ref 17, the whole spreading process can be subdivided into two stages: during the first stage v_+ prevails, and v_- dominates during the second stage of spreading.

Let us consider the second spreading stage. During this stage, the first term in the right-hand side of eq 5 can be neglected, and this equation reduces to

$$\frac{dL}{dt} = \frac{1}{3}\left(\frac{4}{\pi V_d^2\theta}\right)^{1/3}\frac{dV_d}{dt} \tag{7}$$

that after inserting the expression of θ (2) takes the form $dL/dV = L/3V_d$, which can be easily integrated. Its solution is

$$V_d = CL^3 \tag{8}$$

where C is an integration constant. Comparison with eq 2 yields

$$\theta(t) = \theta_e = \text{constant} \tag{9}$$

over the duration of the second stage of the spreading. This conclusion agrees well with our experimental observations (see Results and Discussion) as well as with earlier observations.[17] Note that in the case under consideration, as in ref 17, the constancy of the contact angle has nothing to do with the contact angle hysteresis; there is no hysteresis in the system under consideration. θ_e is not a receding contact angle but forms as a result of a self-regulation of the drop−porous layer system.

Inside the Porous Substrate

The analysis of experimental data shows that the radius of the wetted region inside the porous layer is proportional to l^3. If the drop base (Figure 1) is assumed to be a point source of liquid, then the shape of the wetted area inside the porous substrate is a hemisphere with an increasing radius and a constant *effective* contact angle $\psi(t) = \pi/2$. Obviously a "point source" assumption is too simple an approximation, as both radii, $l(t)$ and $L(t)$, are of the similar size. Yet, it would help to understand the essence of the process. Hence, let us assume that the wetted region inside the porous substrate is a spherical cap form with changing effective contact angle $\psi(t)$ (Figure 1).

Let $V_p = (V_0 - V_d)/m$, where V_p is the volume of the liquid inside the porous substrate at time t, V_0 is the initial volume of the drop, and m is the porosity. Under the above assumption, the liquid volume in the porous substrate, V_p, can be expressed as (Figure 1)

$$V_p = \frac{\pi}{3} l^3 \frac{(1-\cos\psi)^2(2+\cos\psi)}{\sin^3\psi} \tag{9}$$

where l is the radius of the wetted circle on the outer surface of the porous substrate. Equation 9 enables us to calculate the time evolution of ψ using the experimental data.

Experimental Section

Silicone oils S5 (viscosity 0.05 P), S100 (viscosity 1.0 P), and S500 (viscosity 5.0 P) purchased from Brookfield Engeneering Laboratories Inc. (Middleboro, MA) were used in the spreading experiments. Glass filters, J. Bibby Science Products, Ltd., and metal filters, Sintered Products, Ltd, both purchased from Claremont Ltd. (Broseley, U.K.), were used as porous substrates. The diameters of glass filters were 5.0, 2.9, and 2.9 cm, and their thicknesses were 2.5 , 1.9, and 2.2 mm, respectively. The diameter

Table 1. Characteristics of Porous Substrates and Drops Used

material, fig., symbol	porosity	av pore size, mm	η, P	V_0, mL	t^*, s	L_m, mm	l^*, mm	θ_m, grad	Ψ^*, grad
glass, Figure 3, △	0.53	4.7	0.05	5.0	0.64	2.42	3.10	25.8	38
glass, Figure 3, □	0.53	4.7	1	5.9	12.0	2.30	3.20	24.4	39
glass, Figure 3 ○	0.53	4.7	5	8.2	60.0	2.58	3.50	23.6	42
cupro-nickel, Figure 4, □	0.32	26.1	5	8.2	15.7	2.38	3.20	35.0	52
glass, Figure 4, ○	0.31	26.8	5	6.8	18.52	2.40	3.20	25.5	44
glass, Figure 5, □	0.56	3.7	5	8.0	36.0	2.53	3.2	21.5	30
glass, Figure 5, ○	0.31	26.8	5	6.8	18.52	2.40	3.20	25.5	44

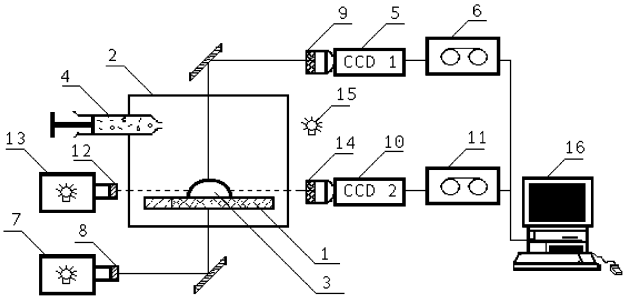

Figure 2. Sketch of the experimental setup: (1) wafer; (2) sample chamber; (3) tested drop; (4) dosator; (5, 10) CCD-cameras; (6, 11) VCRs; (7, 13) illuminators; (8, 9, 12, 14) interferential light filters (8 and 9 with wavelength 520 nm, and 12 and 14 with wavelength 640 nm).

of metal filters was 5.6 cm, and their thickness was 1.9 mm. Pore size distribution and permeability of membranes were tested using the Coulter Porometer II (Coulter Electronic Ltd, Luton, U.K.).

Glass filters with three different pore size distributions were used. The average pore sizes were 3.7, 4.7, and 26.8 μm, respectively; their porosities were 0.56, 0.53, and 0.31, respectively. The permeabilities of the same membranes were 1.8 ; 1.9 and 11.5 L min^{-1} cm^{-2} (air flux, transmembrane pressure 0.1 bar). Metal filters (Cupro-Nickel) had an average pore size of 26.1 μm and porosity of 0.32. The porosity of filters was measured using the difference in the weight of the filters saturated with oil and the dry filters. Filters were dried during 3−5 h at 95 °C and then stored in a dry atmosphere prior to the spreading experiments. All relevant information and values are summarized in the Table 1.

Figure 2 shows a schematic description of the setup. The time evolution of the radius of the drop base, $L(t)$, the dynamic contact angle, $\theta(t)$, and the radius of the wetted circle on the surface of the porous substrate, $l(t)$, were monitored. The porous substrate (1) (Figure 2) was placed in a thermostated and hermetically closed chamber (2) where zero humidity and fixed temperature (20 ± 0.5 °C) were maintained. To prevent temperature fluctuations, the chamber was made from brass. In the chamber walls, several channels were drilled which were used for pumping a thermostating liquid. The chamber was equipped with a fan. The temperature was monitored by a thermocouple. A box with a dried silica gel was used to keep zero humidity inside the chamber. Droplets of the liquid under investigation (3) were placed onto the dry porous substrate by a dosator (4). The distance from the porous substrate to the tip of the dosator ranged from 1 to 3 mm in different experiments. The drop volume was set by the diameter of a disposable capillary of the dosator in the range of 4−8 μL. The chamber was equipped with optical glass windows for observation of both the shape and the size of the spreading drops; a side view and a top view were carried out. Two CCD cameras and two video recorders were used for storing the data as the spreading process went on. Monochromatic light of different colors was used for side and top views to eliminate spurious effects. An optical circuit for top view (illuminator (7) and camera (5)) was equipped with interferential light filters (8 and 9) with wavelength 520 nm. A side view circuit (illuminator (13) and camera (10)) was equipped with filters (12 and 14) with wavelength 640 nm. Such arrangement suppresses illumination of the CCD camera (2) by the scattered light from the membrane and, hence, results in higher precision of the measurements. Automatic processing of images was carried out using image grabber LG-3 and image software Scion Image made by Scion Corporation (Frederick, MD). The amount of time in the processing ranged from 0.04 to 5 s in different experiments; the pixel size in an image was 0.013−0.018 mm in different runs. All porous substrates before experiment were placed for half an hour in a KOH aqueous solution inside an ultrasonic bath, rinsed out by plenty of Milli-Q water (Milli-Q water system, made by Millipore S.A., France) in an ultrasonic bath, and then they were dried for 2 h in an 110 °C dry atmosphere. Porous substrates were stored in a dry atmosphere before starting the experiments.

Experiments were carried out in the following order: the dry porous substrate was placed in the dry atmosphere chamber and left there for 15−30 min, a light pulse produced by a flash gun was used to synchronize the time instant in both video recorders when the drop started to spread; a droplet of silicone oil was placed onto the porous substrate. Each run was carried out until the complete imbibition of the drop into the porous substrate took place.

Results and Discussion

According to our observations, the whole spreading process can be subdivided into two stages (see, e.g., Figure 3, parts a and b): the first stage, when the drop spreads until the maximum radius (L_m) of the drop base is reached, which is followed by the second stage, when the drop radius decreases. Over the duration of the first stage, the imbibition front inside the membrane grows slightly ahead of the drop spreading front. Subsequently, the drop base starts to shrink until the drop completely disappears and the imbibition front grows until the end of the process. Examples of the time evolution of the radius of the drop base and the radius of the wetted circle on the surface of the porous substrates are presented in Figure 3a,b, Figure 4a, and Figure 5a.

In all experiments, the drops remained spherical over the whole spreading process. This was cross-checked by reconstructing the drop profiles at different time instants of spreading, fitting those drop profiles by a spherical cap: $h = z_{center} + (R^2 - (r - r_{center})^2)^{1/2}$, where (r_{center}, z_{center}) is the position of the center of the sphere and R is the radius of the sphere. r_{center}, z_{center}, and R are used as fitting parameters. The Levenberg−Marquardt algorithm was used for fitting. In all cases, the reduced Chi-square value was found to be smaller than 10^{-4}. The fitted parameter R gives the radius of curvature of the spreading drops at different times.

The wetted area on the surface of the porous substrate was always circular. Drops remained in the center of this circle over the whole duration of the spreading process. No deviations from cylindrical symmetry or instabilities were detected.

The spherical form of the spreading drop allows measuring the evolution of the dynamic contact angle of the spreading drops. In all cases, the dynamic contact angle decreased very fast during the first spreading stage and remained constant during the second spreading stage. This constant value of the contact angle is denoted below as θ_e.

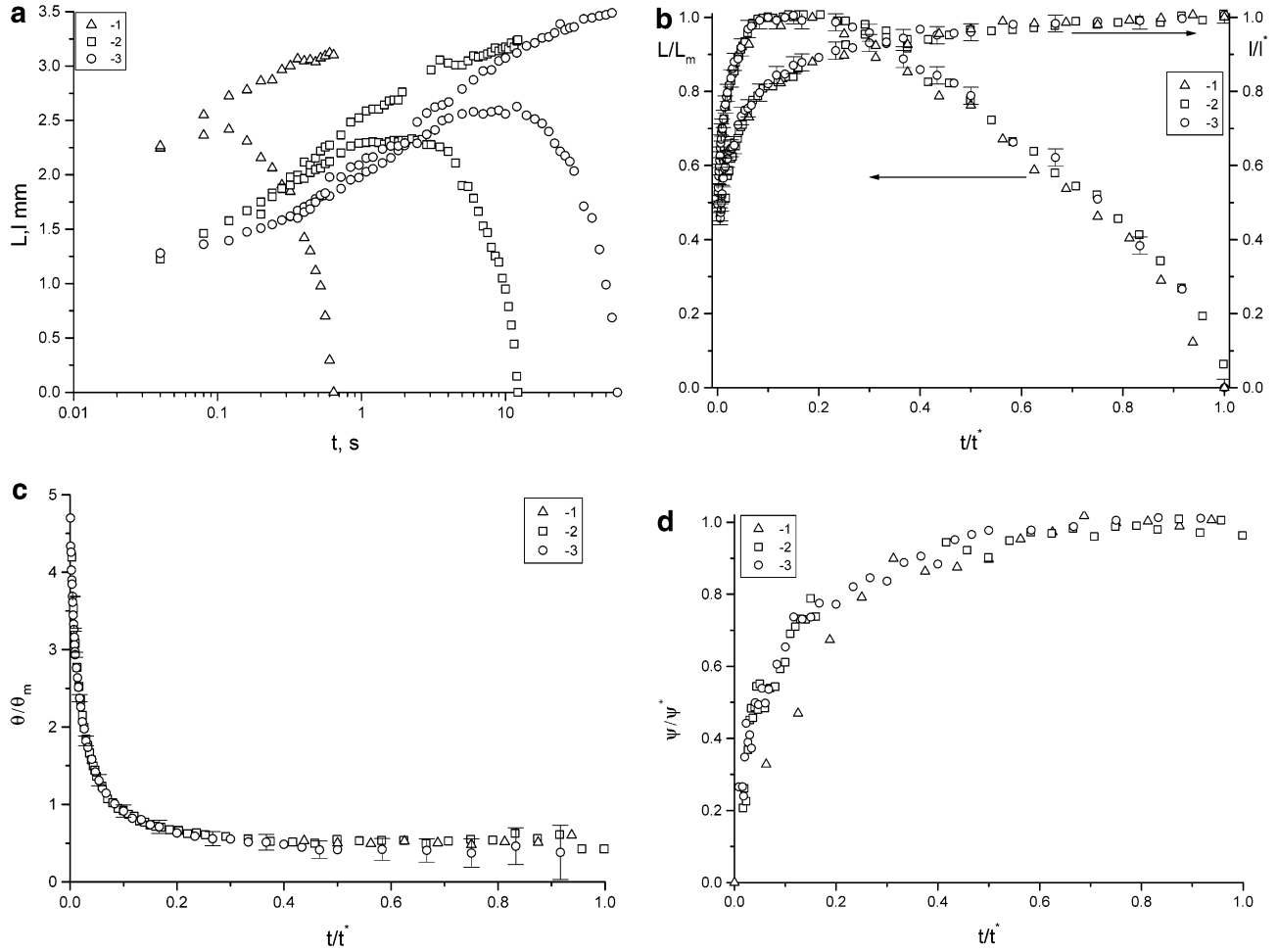

Figure 3. Spreading of different silicone oils over the same dry porous glass filter. Glass porous filter: porosity 0.53, average pore size 4.7 μm, permeability 1.9 l/min/cm^2. Key: (1) silicone oil $\eta = 0.05$ P; (2) silicone oil, $\eta = 1$ P; (3) silicone oil, $\eta = 5$ P (see insets). (a) The same symbols show the evolution of $l(t)$ and $L(t)$ with time: (lower parts) $L(t)$, radius of the base of the spreading drop; (upper parts) $l(t)$, radius of the wetted circle on the surface of the porous glass filter in dimensional form; (b) the same data as in Figure 3a using appropriate dimensionless coordinates. L_m, the maximum value of the radius of the drop base; l^*, the maximum value of the radius of the wetted circle on the surface of the glass fiilter; t^*, the total duration of the process (see Table 1). (c) Dynamic contact angle versus time in dimensionless units. θ_m, dynamic contact angle value at the time when the maximum value of the radius, L_m, of the drop base is reached (see Table 1). (d) Evolution of the effective contact angle inside the porous glass filters with the dimensionless time. ψ^* is the maximum value of the effective contact angle (see Table 1).

Examples of the evolution with time of the dynamic contact angle are presented in Figure 3c, Figure 4b, and Figure 5b. These figures show that the dynamic contact angle decreases during the first spreading stage when the radius of the drop base grows up to its maximum value, L_m. Within experimental error, the dynamic contact angle remains unchanged during the second spreading stage.

Spreading of Silicone Oils Drops of Different Viscosity over the Same Glass Filter (Figure 3). Figure 3 presents experimental results on the spreading of silicone oil drops of different viscosity over identical glass filters. Silicone oils S5, S100, and S500 were used in these spreading experiments. The diameter of the glass filter was 2.9 cm, its thickness was 1.9 mm, its porosity was 0.53, and its average pore size was 4.7 mm.

In Figure 3, △ represents the spreading of the silicone oil S5 (drop volume $V_0 = 5.0$ mL, the maximum radius of the drop base $L_m = 2.42$ mm, the maximum (final) radius of the wetted circle on the outer surface of the glass filter $l^* = 3.10$ mm, and the total duration of the spreading $t^* = 0.64$ s), □ represents the spreading of the silicone oil S100 (drop volume $V_0 = 5.9$ mL, the maximum radius of the drop base $L_m = 2.30$ mm, the maximum (final) radius of the wetted circle on the outer surface of the glass filter $l^* = 3.20$ mm, and the total duration of the spreading $t^* = 12.0$ s), and ○ represents the spreading of the silicone oil S500 (drop volume $V_0 = 8.2$ mL, the maximum radius of the drop base $L_m = 2.58$ mm, the maximum (final) radius of the wetted circle on the outer surface of the glass filter $l^* = 3.50$ mm, and the total duration of the spreading $t^* = 60.0$ s).

In Figure 3a the time evolution of both the radius of the base of the spreading drops and the radius of the wetted circle on the outer surface of the glass filter for silicone oils of different viscosity are presented using experimental data in dimensional form. Figure 3a shows that the kinetics of the spreading, and the imbibition varies for drops of different size and different viscosity. Consequently, the total duration of the spreading process, the maximum radius of the drop base, and the radius of the wetted circle on the outer surface of the glass filter vary considerably. However, if as in ref 17 we rescale quantities L/L_m, l/l^* and t/t^*, then all experimental data fell into two universal curves as Figure 3b shows.

According to ref 17, the evolution of reduced dynamic contact angle, θ/θ_m, with the dimensionless time, t/t^*, should be universal. Here, θ_m is the maximum value of the dynamic contact angle, which is reached when the radius of the drop base reaches its maximum value (the end of the first stage of spreading). The same procedure

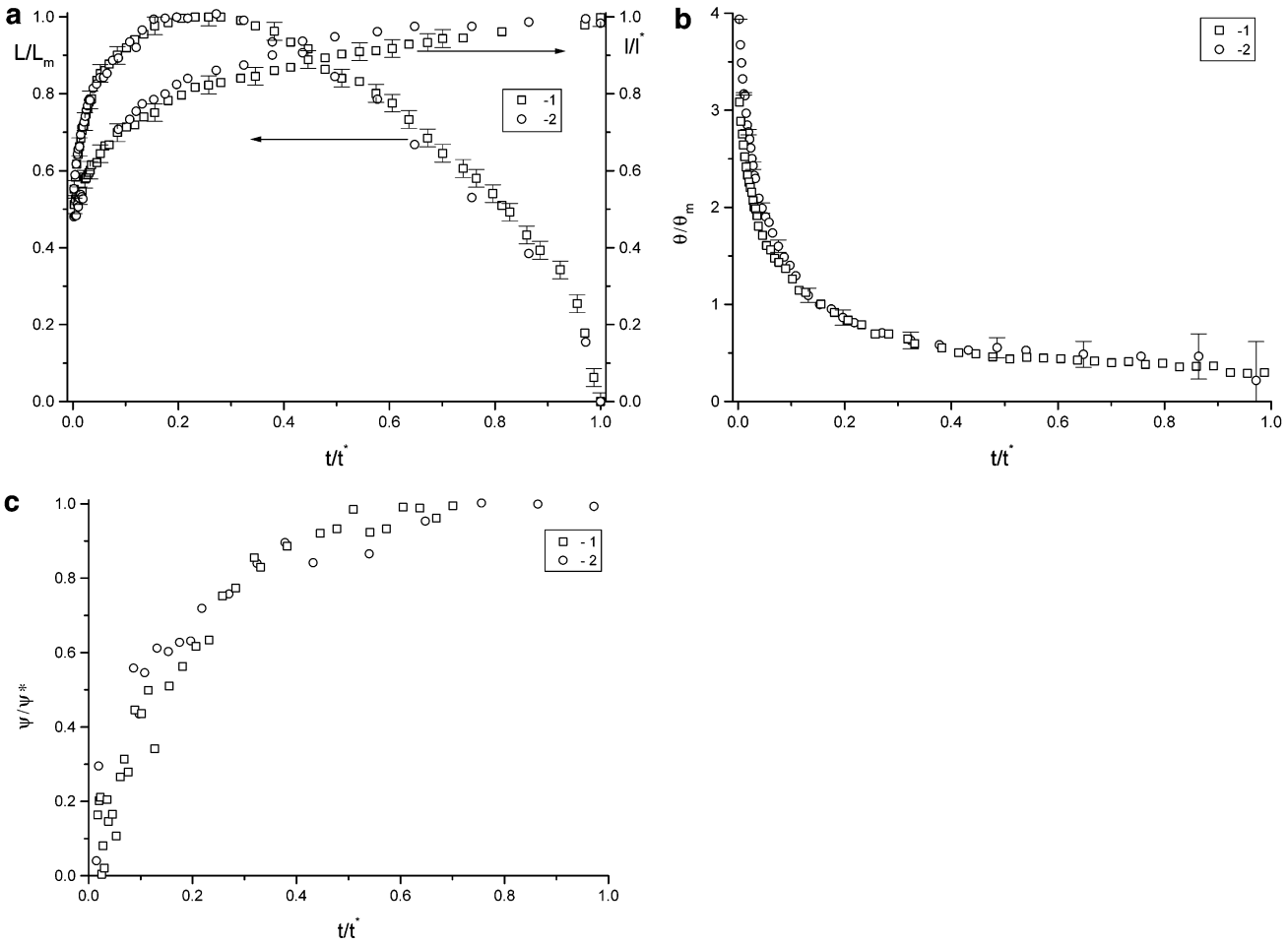

Figure 4. Spreading of silicone oil ($\eta = 5$ P) over dry porous glass and metal filters (radii in reduced co-ordinates): (1) metal filter, porosity 0.32, average pore size 26.1 μm (see insets); (2) glass filter, porosity 0.31, average pore size 26.8 μm (see insets). L_m the maximum value of the radius of the drop base; l^* maximum value of the radius of the wetted circle on the surface of the glass filter; t^*, the total duration of the process (see Table 1). (a) radii in reduced coordinates; (b) dynamic contact angle versus time in dimensionless units θ_m is the dynamic contact angle value at the time when the maximum value of the radius of the drop base, L_m, is reached (see Table 1). evolution of the effective contact angle inside the porous filters with the relative time. ψ^* is the maximum value of the effective contact angle (see Table 1).

in the case of spreading over thick porous substrates is used below. In Figure 3c, the reduced dynamic contact angle, θ/θ_m, is plotted versus the dimensionless time t/t^*.

This plot shows that (i) all three experimental curves fall into a single universal curve and (ii) the dynamic contact angle remains constant during the second spreading stage as theory predicts.

In Figure 3d the evolution of the relative effective dynamic contact angle, ψ/ψ^*, inside the porous glass filter with the dimensionless time is presented. Noteworthy is that in all three cases all data follow a single universal curve.

These three experimental runs show that the spreading behavior of drops of different viscosities and volumes on the same thick porous substrate is identical if appropriate dimensionless coordinates are used.

Spreading of Silicone Oil Drops over Filters with Similar Properties but Made of Different Materials (Figure 4). In this series of experiments, the spreading of drops of the same silicone oil S500 over different substrates was studied. We wanted to check if the universal behavior found in the previous case remains valid even when different porous substrates made of different material, e.g., glass and metal filter, are used.

In Figure 4, □ represents the spreading of the silicone oil S500 (drop volume $V_0 = 8.2$ mL, the maximum radius of the drop base $L_m = 2.38$ mm, the maximum radius of the wetted circle on the outer surface of the porous substrate $l^* = 3.20$ mm, the total duration of the spreading $t^* = 15.7$ s over the metal filter (Cupro-Nickel) with diameter 5.6 cm, thickness 1.9 mm, average pore size 26.1 μm, porosity 0.32) and ○ represents the spreading of the silicone oil S500 (drop volume $V_0 = 6.8$ mL, maximum radius of the drop base $L_m = 2.40$ mm, maximum radius of the wetted circle on the outer surface of the porous substrate $l^* = 3.20$ mm, the total duration of the spreading $t^* = 18.52$ s over the glass filter with diameter 2.9 cm, thickness 2.2 mm, porosity 0.31, and average pore size 26.8 mm).

Figure 4a presents the dependence of the dimensionless radius of the drop base (left ordinate) and that of the dimensionless radius of the wetted circle on the outer surface of the porous substrate (right ordinate) on the dimensionless time. Figure 4b presents the dependence of the relative dynamic contact angle on the dimensionless time. Figure 4c presents the dependence of the effective dynamic contact angle inside the porous substrate on the same dimensionless time.

The curves show that the spreading of drops of different size on porous substrates made of different materials with, however, similar porosity and average pore size, fall on universal curves if, as in the previous case, the same

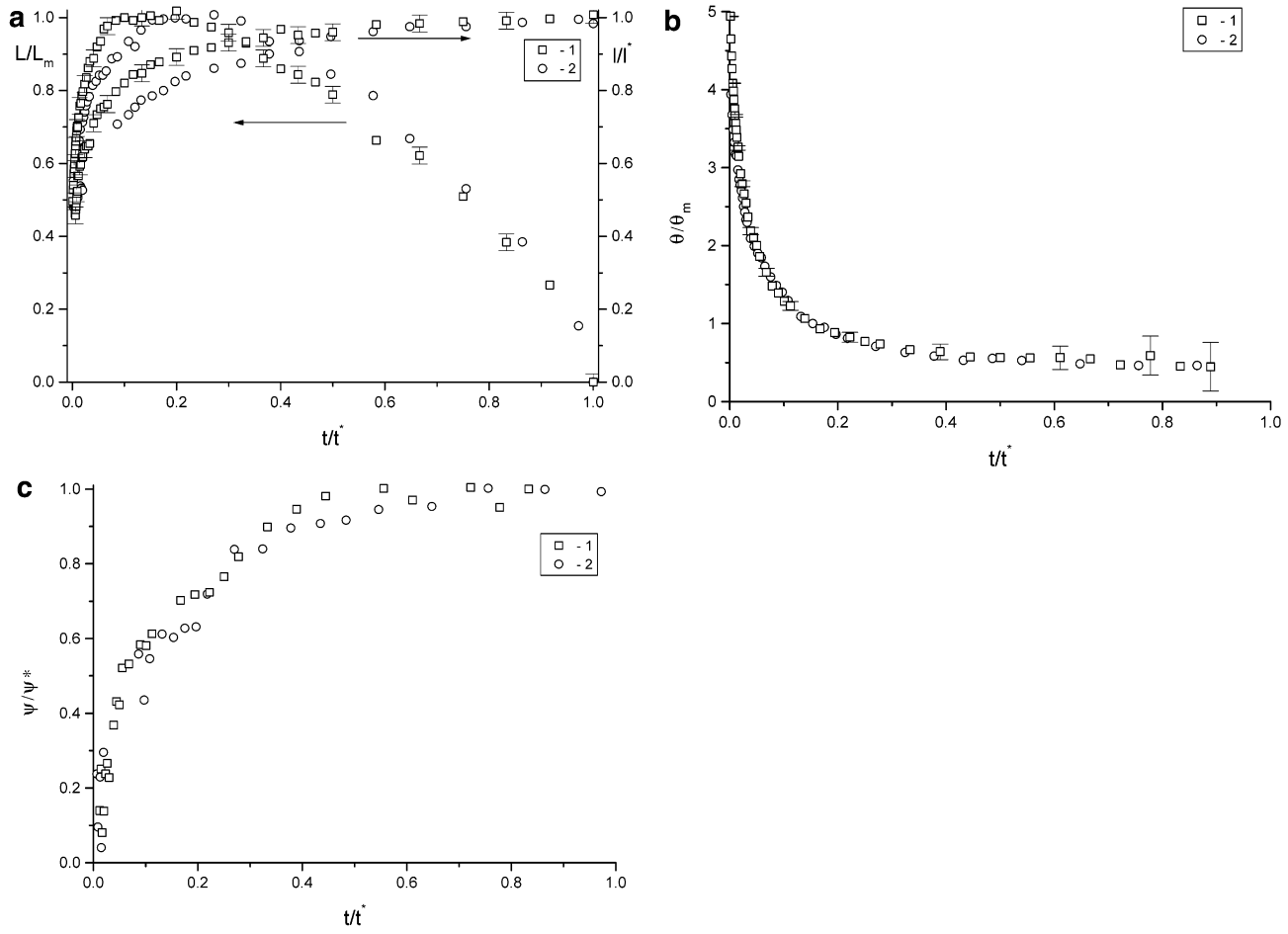

Figure 5. Spreading of silicone oil ($\eta = 5$ P) over different dry glass filters. (1) glass filter, porosity 0.56, pore size 3.7 μm (see insets); (2) glass filter, porosity 0.31, pore size 26.8 μm (see insets). (a) Radii of spreading in reduced co-ordinates. L_m is the maximum value of the radius of the drop base; l^* is the maximum value of the radius of the wetted circle on the surface of the glass filter; t^* is the total duration of the process (see Table 1). (b) Dynamic contact angle versus time in dimensionless units. θ_m is the dynamic contact angle value at the time when the maximum value of the radius of the drop base, L_m, is reached (see Table 1). (c) Evolution of the effective contact angle inside the porous filters with time in dimensionless units. ψ^* is the maximum value of the effective contact angle (see Table 1).

dimensionless coordinates are used. Thus, the universal spreading behavior over porous substrates does not depend on the material of the porous substrate.

Spreading of Silicone Oil Drops with the Same Viscosity ($\eta = 5$ P) over Glass Filters with Different Porosity and Average Pore Size (Figure 5). In this section, the spreading of silicone oil drops with the same viscosity over glass filters with different porosity and average pore size is investigated to check if the universal behavior found in two previous sections is still applicable.

In Figure 5, □ represents the spreading of silicone oil S500 (drop volume $V_0 = 8.0$ mL, maximum radius of the drop base $L_m = 2.53$ mm, maximum radius of the wetted circle on the surface $l^* = 3.20$ mm, the total duration of the spreading $t^* = 36.0$ s over the glass filter with diameter 5.0 cm thickness 2.5 mm, porosity 0.56, and average pore sizes 3.7 mm) and ○ represents the spreading of the silicone oil S500 (drop volume $V_0 = 6.8$ mL, maximum radius of the drop base $L_m = 2.40$ mm, maximum radius of the wetted circle on the outer surface of the glass filter $l^* = 3.20$ mm, the total duration of the spreading $t^* = 18.52$ s over the glass filter with diameter 2.9 cm, thickness 2.2 mm, porosity 0.31, and average pore sizes 26.8 mm).

Figure 5, parts b and c, shows that the relationships between the relative dynamic contact angle, θ/θ_m, and the effective dynamic contact angle inside the porous substrate, ψ/ψ^*, on the dimensionless time, t/t^*, again exhibit universal behavior. However, the dependence of the dimensionless radius of the drop base, L/L_m, and that of the dimensionless radius of the wetted circle on the surface of the porous substrate, l/l^*, on the dimensionless time, t/t^*, deviate from universal behavior during first spreading stage. The duration of the first stage, when the drop base increases with time and reaches its maximum value, is shorter in the case of the spreading of silicone oil drops over the glass filter with a smaller average pore size than in the case of the spreading over the glass filter with a larger average pore size (Figure 5a).

In conclusion, we can safely say that the spreading behavior over porous substrates is mostly, if not all, determined by the porosity and the average pore size of the porous substrate and differs if these two characteristics are different.

Conclusions

Experiments were carried out on the spreading of small silicone oil drops (capillary regime of spreading) over various dry thick porous substrates (permeable in both normal and tangential directions). The time evolution of the radii of both the drop base and the wetted region on the surface of the porous substrate was monitored. It has been shown that the overall duration of the spreading process can be divided into two stages: a first stage, when

the drop base is grown until a maximum value is reached, and a second stage, when the drop base shrinks. It has been observed that the dynamic contact angle remained constant during the second spreading stage. This fact is supplied by a heuristic argument and has nothing to do with hysteresis of contact angle, as there is no hysteresis in our system. Using appropriate scales, the dimensionless radius of the drop base, the radius of the wetted circle on the surface of the porous substrate, the dynamic contact angle, and the effective contact angle inside the porous substrate have been plotted using a dimensionless time.

Our experimental data show that the spreading of silicone oil drops over dry thick porous substrates exibits a universal behavior if (i) porous substrates made of different materials with, however, similar porosity and average pore size are used and (ii) if appropriate dimensionless coordinates are introduced to depict the data. However, if porous substrates with different porosity and average pore size are used, the dynamic of both the radius of the drop base, L/L_m, and the radius of the wetted circle on the outer surface of the porous filter, l/l^*, behave differently during the spreading process. Yet both the relative dynamic contact angle, θ/θ_m, and the effective contact angle inside the porous substrate, ψ/ψ^*, show universal behavior.

List of Symbols

Latin

C	integration constant
h	drop profile
L	radius of the drop base
l	radius of the wetted circle on the outer surface of the porous substrate
m	porosity
p	pressure
R	radius of a spherical segment inside the porous substrate
r, z	coordinate system
t	time
V	volume
v	velocity

Greek

η	viscosity
θ	dynamic contact angle
ψ	effective dynamic contact angle inside the porous substrate

Subscripts

0	initial value
d	drop
center	center of the sphere
m	corresponds to the moment when the drop base reaches its maximum value
p	porous layer
e	marks the constant value of the dynamic contact angle over the duration of the second stage of the spreading
+	expansion
−	shrinkage

Superscripts

*	maximum value

Acknowledgment. The research reported here has been supported by Grant GR/R 07578 from the U.K. Engineering and Physical Sciences Research Council and by Grant PB 96-599 from the Spanish Ministerio de Ciencia y Tecnologia.

LA025759Y